Ann Nucl Med (2017) 31:437–453
DOI 10.1007/s12149-017-1182-3

REVIEW ARTICLE

Pictorial review of ^{18}F-FDG PET/CT findings in musculoskeletal lesions

Mana Ishibashi[1] · Yoshio Tanabe[1] · Shinya Fujii[1] · Toshihide Ogawa[1]

Received: 3 April 2017 / Accepted: 27 May 2017 / Published online: 5 June 2017

Abstract We herein reviewed ^{18}F-fluoro-2-deoxyglucose (^{18}F-FDG) positron emission tomography (PET)/computed tomography (CT) findings in a number of musculoskeletal lesions including malignant tumors, benign tumors, and tumor-like lesions with correlations to other radiographic imaging modalities, and described the diversity of the ^{18}F-FDG PET/CT findings of this entity. Malignant primary musculoskeletal tumors are typically ^{18}F-FDG avid, whereas low-grade malignant tumors show mild uptake. Benign musculoskeletal tumors generally show a faint uptake of ^{18}F-FDG, and tumor-like conditions also display various uptake patterns of ^{18}F-FDG. Although musculoskeletal tumors show various uptakes of ^{18}F-FDG on PET/CT, its addition to morphological imaging modalities such as CT and MRI is useful for the characterization and differentiation of musculoskeletal lesions.

Keywords FDG · PET/CT · Bone tumor · Soft tissue tumor

Introduction

Positron emission tomography (PET)/computed tomography (CT) is a molecular imaging technique that uses positron-emitting radionuclides to image the molecular interactions of biological processes. Most PET imaging studies in malignant tumors are performed using ^{18}F-fluoro-2-deoxyglucose (^{18}F-FDG), which is a tracer of increased intracellular glucose metabolism and, thus, is taken up by malignant tumors. ^{18}F-FDG accumulation reflects the rate of glucose utilization in a tissue, since ^{18}F-FDG is transported into a tissue by the same mechanisms of glucose transport and trapped in the tissue as FDG-6-phosphate, which cannot serve as a substrate for further metabolism of glycolysis or glycogen storage. More aggressive tumors may have increased rates of glycolysis in comparison to less aggressive tumor and normal tissues; therefore, ^{18}F-FDG PET has been used for evaluation of aggressiveness, tumor grading, and prognostication. Similar to other malignancies, malignant musculoskeletal tumors also exhibit an increased rate of glycolysis and a strong uptake of ^{18}F-FDG, whereas low-grade malignant tumors show mild uptake. Benign musculoskeletal tumors generally show mild uptake, while tumor-like conditions display various uptake patterns of ^{18}F-FDG. These lesions need to be differentiated from malignant tumors including metastatic bone tumors in cancer patients. Therefore, a clearer understanding of the diversity of ^{18}F-FDG PET/CT findings on musculoskeletal lesions is important for the proper interpretation of ^{18}F-FDG PET/CT in conjunction with CT and magnetic resonance imaging (MRI).

We herein reviewed ^{18}F-FDG PET/CT findings in a number of musculoskeletal lesions including malignant tumors, benign tumors, and tumor-like lesions with correlations to other radiographic imaging modalities such as CT and MRI, and described issues related to the ^{18}F-FDG PET/CT findings of various musculoskeletal lesions (Table 1).

✉ Mana Ishibashi
ishibashi-ttr@umin.ac.jp

[1] Division of Radiology, Department of Pathophysiological and Therapeutic Science, Faculty of Medicine, Tottori University, 36-1 Nishicho, Yonago 683-8504, Japan

Table 1 ^{18}F-FDG accumulation in musculoskeletal tumors

^{18}F-FDG uptake	Mild	Moderate	Strong
Malignant tumors			Osteosarcomas
			DSRCT
			Undifferentiated sarcomas
		Leiomyosarcomas	
		Malignant peripheral nerve sheath tumors	
	Rhabdomyosarcomas		
	Liposarcomas		
	Chondrosarcomas		
	Chordomas		
Benign tumors or lesions	Enchondromas		
	Hemangiomas		
	Neurogenic tumors		
	Fat necrosis		
			Langerhans cell histiocytosis

DSRCT desmoplastic small round cell tumors, *undifferentiated sarcoma*s undifferentiated/unclassified sarcomas

Malignant tumors

Osteosarcomas

Osteosarcomas are the most common primary malignant bone tumors in children and adolescents and are also regarded as the second most common primary bone tumor following plasma cell myeloma in adults [1, 2]. Osteosarcomas are classified into several subtypes based on their locations within the bone, the cell type, histological grade, and age at presentation, and its subtypes vary in their clinical presentation and features, radiographic findings, and prognosis [1, 2]. These tumors most commonly occur in the distal end of the femur and the proximal ends of the tibia and humerus, and less commonly in the pelvic bone. The potential of osteosarcomas to metastasize is very high, particularly to the lungs [1].

Osteosarcomas have an increased rate of glycolysis like many other malignancies, and consequently demonstrate strong uptake of ^{18}F-FDG [1–3] (Fig. 1). ^{18}F-FDG PET/CT provides detailed information on tumor staging, treatment responses, and the monitoring of recurrence [3–5]. Tumor staging and histological grades play an important role in treatment strategies and the prediction of prognoses [6, 7]. Previous studies demonstrated that the maximum standardized uptake value (SUVmax) correlated with histological grades and increased ^{18}F-FDG uptake in parallel with tumor grades, and also that ^{18}F-FDG PET has the capacity to differentiate between low- and high-grade osteosarcomas [3, 5, 8]. Other studies proposed that ^{18}F-FDG PET-guided biopsy contributes to accurate grading and prognostication [9, 10]. ^{18}F-FDG PET/CT is also useful for the non-invasive assessment of treatment responses after chemotherapy [11, 12] (Fig. 1). Moreover, ^{18}F-FDG PET/CT has demonstrated high diagnostic accuracy for the detection of recurrence in the follow-up of patients with osteosarcomas [13, 14]. Quartuccio et al. reported that ^{18}F-FDG PET/CT was more accurate than conventional imaging for the detection of recurrence with diagnostic benefits [14]. Furthermore, in patients with metallic prostheses, imaging artifacts often hamper CT and MRI findings [2].

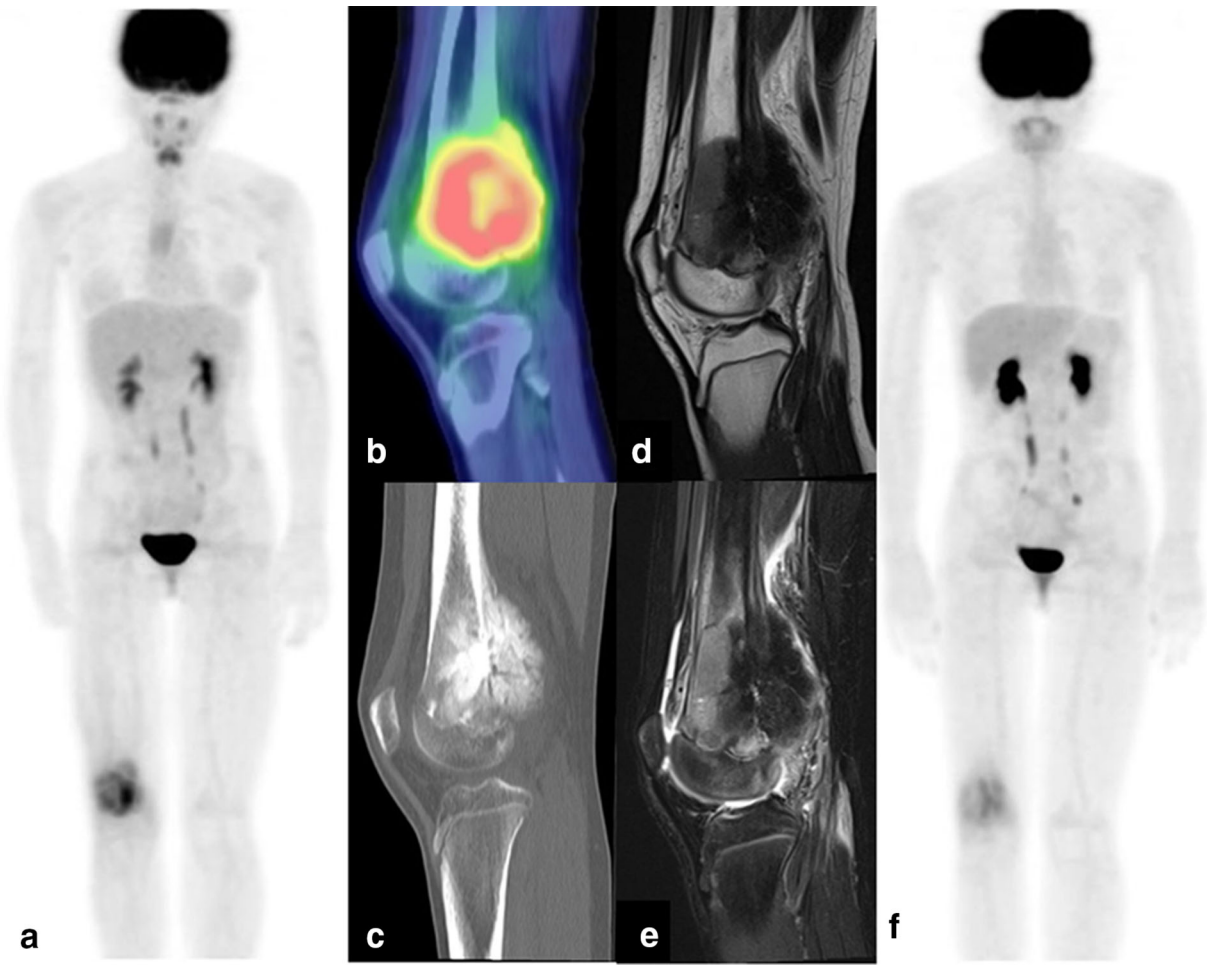

Fig. 1 An 11-year-old female with osteosarcoma (Grade 2) of the right femur. **a**, **b** ^{18}F-FDG PET/CT and MIP images demonstrate strong uptake with SUVmax of 6.1. **c** CT shows an osteolytic and osteoblastic tumor of the distal femur. **d**, **e** MRI reveals heterogeneous hypointensity on T1WI and hyperintensity on fat-suppressed T2WI. **f** ^{18}F-FDG PET/CT MIP image after chemotherapy shows mild uptake with SUVmax of 3.1, consistent with the treatment response

CT shows tumors as densely mineralized lesions resulting from osteoblastic formations in most cases [15]. MRI displays tumors as hypointensity on T1-weighted images (T1WI), and heterogeneous hyperintensity on T2-weighted images (T2WI). Ossified formations show signal voids on all sequences. Gadolinium (Gd)-enhanced T1WI shows heterogeneous enhancements [15].

Chondrosarcomas

Chondrosarcomas are malignant cartilaginous tumors that account for approximately 20% of all primary malignant bone tumors and are the third most common tumors after myelomas and osteosarcomas [16]. Most patients are adults, and its peak incidence is between 50 and 70 years of age [1]. It is more common in males than in females. This tumor most commonly occurs in the pelvis and femur [16]. Conventional chondrosarcomas and clear cell chondrosarcomas are often low- to intermediate-grade tumors that are not very aggressive and mostly remain in one location, whereas dedifferentiated and mesenchymal chondrosarcomas are high-grade tumors that exhibit aggressive behavior and are more likely to spread [16]. Most chondrosarcomas are locally aggressive, non-metastatic, low-grade tumors [2].

^{18}F-FDG PET demonstrates mild to moderate uptake in parallel with tumor grades [17–19] (Figs. 2, 3) and may predict prognostication in patients with chondrosarcoma [17, 18]. A previous study reported that the mean SUVmax was 3.4 for grade I, 5.4 for grade II, and 7.1 for grade III [17].

CT shows these tumors as a soft tissue attenuation mass with internal calcification and the destruction of bone [16]. MRI reveals these tumors as hypo- to intermediate intensity on T1WI and as strong hyperintensity on T2WI with a lobular growth pattern. Gd-enhanced T1WI shows

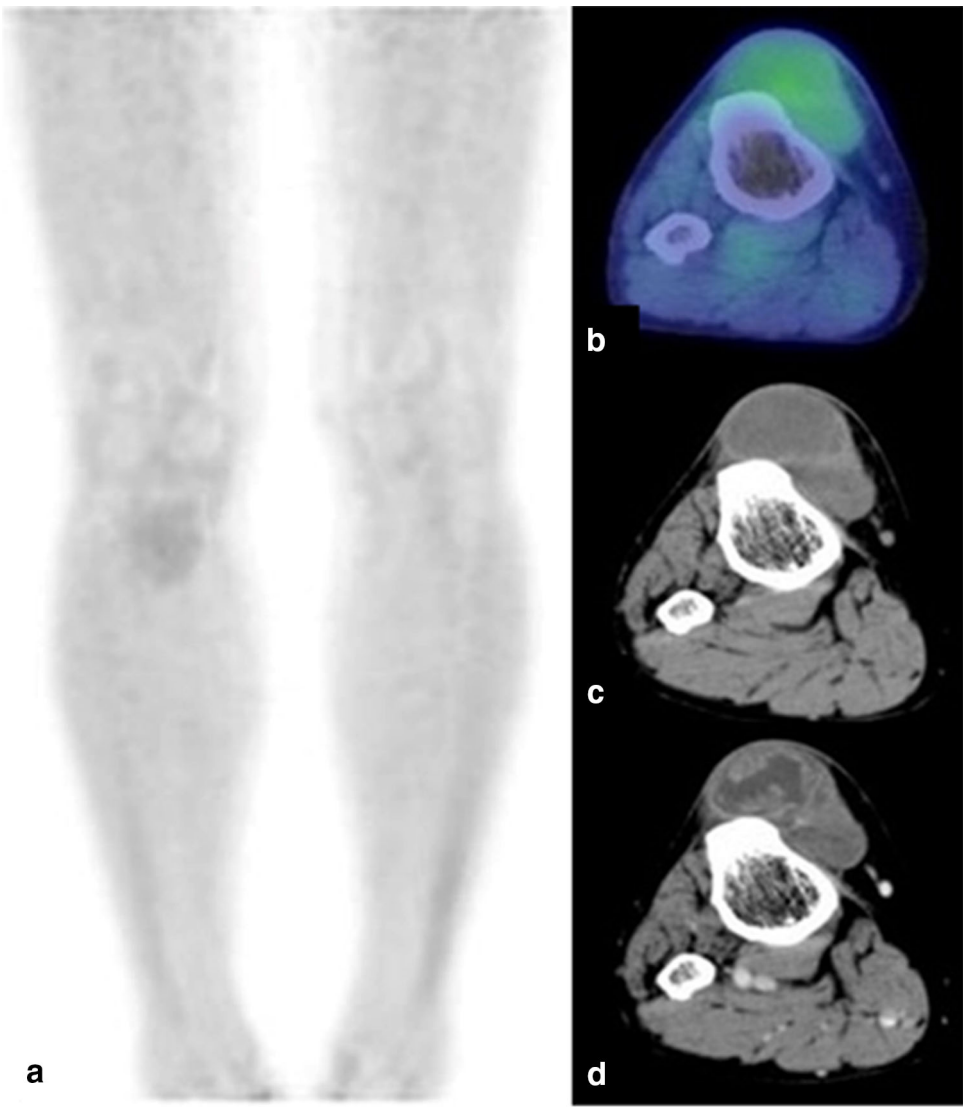

Fig. 2 A 69-year-old female with periosteal chondrosarcoma (Grade 2) of the right tibia. **a**, **b** ^{18}F-FDG PET/CT and MIP images demonstrate mild uptake with SUVmax of 1.8. **c**, **d** CT shows a low attenuation mass with heterogeneous, peripheral-dominant enhancement

heterogeneous, moderate to strong septal and peripheral rim enhancements corresponding to the fibrovascular septa [16].

Chordomas

Chordomas are malignant bone tumors that arise from the remnants of the primitive notochord, which is locally aggressive and slow growing. The tumor occurs at the end of the axial skeleton, most commonly at the sacrococcygeal level and skull base [20]. These tumors typically manifest between 40 and 70 years of age and there is a slight male predominance [20].

^{18}F-FDG PET shows heterogeneously mild to moderate uptake (Fig. 4), and the SUVmax of chordomas was reported to vary between 2.1 and 5.8 in previous case reports and clinical studies [20–23]. Slow growth and histological findings of the relatively low metabolic activity of abundant mucin and low cellularity may explain the mild uptake of ^{18}F-FDG in spite of malignant tumors [21]. In a previous case report, since the uptake of ^{18}F-FDG by recurrent chordomas was greater than that of the initial tumors, ^{18}F-FDG PET contributes to the detection of recurrence by chordomas [20].

CT shows these tumors as well-circumscribed, destructive lytic, and expansile soft tissue masses with irregular intratumoral calcifications [15, 20]. MRI reveals these tumors as hypo- to intermediate intensity with small hyperintense foci on T1WI, and as strong hyperintensity with several septal bands on T2WI. Gd-enhanced T1WI shows moderate and heterogeneous enhancements in most cases [15, 20].

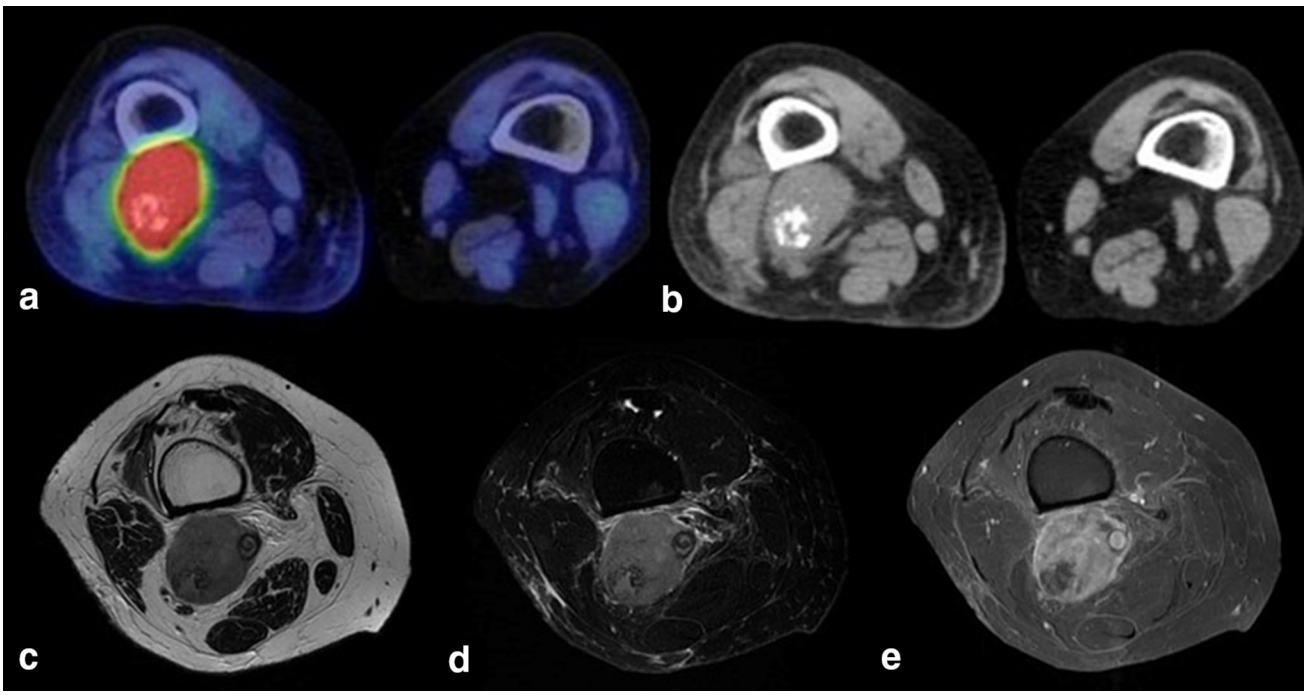

Fig. 3 A 68-year-old female with mesenchymal chondrosarcoma of the right thigh. **a** ^{18}F-FDG PET/CT demonstrates focal strong uptake with SUVmax of 10.4. **b** CT shows a soft tissue attenuation mass with internal calcification. **c**–**e** MRI shows heterogeneous hypointensity on T1WI, hyperintensity on T2WI, and heterogeneous, moderate enhancement with a peripheral rim on Gd-enhanced T1WI

Leiomyosarcomas

Leiomyosarcomas are aggressive soft tissue sarcomas derived from smooth muscle tissues, typically of a uterine, gastrointestinal, or soft tissue origin. Leiomyosarcomas of soft tissue typically develop between 40 and 60 years of age with a twofold higher incidence in females, and more frequently occurs in the retroperitoneum and proximal extremities [24]. The tumor grade is assessed based on histological findings and is considered an important predictor of tumor behavior and outcome. Most soft tissue leiomyosarcomas are of high or intermediate grade and, thus, have a poor prognosis [25].

^{18}F-FDG PET shows strong uptake in correlation with larger and higher-grade tumors (Fig. 5). Punt et al. reported that tumor SUVmax ranged between 2.8 and 26.1, and SUVmax correlated with the tumor grade and size [25]. ^{18}F-FDG PET may differentiate tumor grading and predict tumor behavior [25].

CT generally shows heterogeneous attenuation and commonly displays central low attenuation representing necrosis, while calcification is very rare [24, 26]. MRI reveals these tumors as being isointense to muscle on T1WI and variably hyperintense to muscle on T2WI, with moderate heterogeneous contrast enhancement [26].

Liposarcomas

Liposarcomas are one of the most common soft tissue sarcomas and commonly develop between 30 and 60 years of age [27]. Liposarcomas arise in fat cells in deep soft tissues, such as the buttocks, thighs, lower extremities, and retroperitoneum [27]. Liposarcomas have been divided into four subtypes: well-differentiated, myxoid, dedifferentiated, and pleomorphic liposarcomas [28, 29].

^{18}F-FDG PET demonstrates various uptakes in parallel with tumor grades [30]. Low-grade liposarcomas including well-differentiated and myxoid liposarcomas show mild to moderate uptake (Figs. 6, 7), while high-grade tumors show moderate to strong uptake. Brenner et al. showed that, in addition to tumor grades, ^{18}F-FDG PET was also a useful parameter for predicting outcomes in liposarcoma [30]. Another study reported that ^{18}F-FDG PET was significantly more accurate than size-based criteria in assessing histopathological responses to neoadjuvant therapy in patients with high-grade sarcomas including liposarcomas [31]. Furthermore, a previous review described ^{18}F-FDG PET as a useful modality for the detection of local recurrence and grading of recurrent tumors [2].

CT findings reflect histological subtypes, specifically the amount of fat in a mass with heterogeneous attenuation. Low-grade tumors are almost entirely fat attenuation with

thick septa, enhancements, or evidence of local invasion, whereas higher-grade tumors are often devoid of macroscopic fat with a poor definition of adjacent structures due to infiltration or invasion. The likelihood of calcification is threefold higher in these tumors [29]. MRI shows various findings depending on the grade and amount of fatty tissue, similar to CT. Low-grade tumors show almost entirely fat signal intensities with thick septa; therefore, these tumors show hyperintensity on T1WI and T2WI and hypointensity on fat-suppressed T2WI. These features are used to distinguish these tumors from simple lipomas. Myxoid liposarcomas show hypointensity on T1WI and hyperintensity on T2WI, reflecting a high water content, and a small amount of adipose tissue is observed in the septa or as small nodular foci superimposed on the background of myxoid tissue. Pleomorphic liposarcomas are high-grade sarcomatous lesions and typically appear as heterogeneous soft tissue masses; however, small amounts of fat are observed on MRI [27, 29].

Rhabdomyosarcomas

Rhabdomyosarcomas account for more than 50% of soft tissue sarcomas in children [2]. They are found essentially anywhere in the body, but most frequently occur in the head and neck regions (orbit, oro/nasopharynx, and palate) [32].

^{18}F-FDG PET/CT demonstrates moderate to strong uptake, and SUVmax was previously reported to range between 2 and 20 [2, 32–35] (Fig. 8). The role of ^{18}F-FDG PET in the diagnosis, staging, outcome prediction, and assessment of treatment responses and recurrence in patients with rhabdomyosarcomas was reviewed, and ^{18}F-FDG PET/CT has been suggested to provide further benefits in addition to CT and MRI [2, 33].

CT shows these tumors as soft tissue attenuation masses with indistinct margins, adjacent bony erosion, and some enhancement following contrast media [32]. MRI reveals these tumors as isointense to muscle with hyperintensity due to intratumoral hemorrhage on T1WI, and hyperintense to muscle on T2WI, sometimes with heterogeneous intensity. Gd-enhanced T1WI most commonly shows poorly defined margins and diffuse, often prominent heterogeneous enhancement [34].

Desmoplastic small round cell tumors

Desmoplastic small round cell tumors (DSRCT) are a member of the small round cell tumor family of soft tissue sarcomas. DSRCT typically affect adolescents and young adults, with a fourfold higher incidence in males [36]. It has an aggressive course with generally poor survival.

^{18}F-FDG PET/CT demonstrates strong uptake and the SUVmax of DSRCT was previously reported to be higher than 5 [36–38] (Fig. 9). ^{18}F-FDG PET/CT is useful for detecting metastasis and evaluating the progression of disease and treatment responses [36, 37].

CT shows these tumors as soft tissue masses with patchy hypoattenuation foci due to hemorrhagic tumor necrosis and heterogeneous and mild enhancement following contrast media [36, 38]. MRI reveals these tumors as heterogeneous, iso- or hypointensity on T1WI and hyperintensity on T2WI. Gd-enhanced T1WI shows heterogeneous and mild enhancement [38].

Undifferentiated/unclassified sarcomas

In 2013, the World Health Organization (WHO) declassified malignant fibrous histiocytomas (MFH) as a formal diagnostic entity and renamed them as undifferentiated/unclassified sarcomas [39]. These tumors typically occur in adults with the highest incidence being reported between 40 and 60 years of age, and more often present in the lower limbs (thigh), followed by the retroperitoneum and upper limbs [2].

^{18}F-FDG PET/CT demonstrates strong uptake in most cases [1, 2, 40–42] (Fig. 10). Although ^{18}F-FDG PET/CT has not yet been performed to evaluate this tumor because of its rarity, several case reports and reviews have referred to ^{18}F-FDG PET/CT as a valuable tool for detecting the primary site and metastasis [1, 2, 40–42]. Furthermore, ^{18}F-FDG/PET/CT may be useful for treatment assessments after chemotherapy, similar to other ^{18}F-FDG avid sarcomas (Fig. 11).

CT shows these tumors to be similar to the adjacent muscle, with heterogeneous low-attenuation areas if hemorrhage, necrosis, or myxoid material is abundant [43]. MRI reveals these tumors as intermediate intensity, similar to the adjacent muscle on T1WI, and hyperintensity on T2WI with a lobulated margin and hypointense rim, and sometimes as heterogeneous intensity if hemorrhage, calcification, necrosis, or myxoid material is present. Gd-enhanced T1WI shows the prominent enhancement of solid components [43].

Malignant peripheral nerve sheath tumors (MPNST)

Malignant peripheral nerve sheath tumors (MPNST) are the malignant transformation from benign neurogenic tumors, typically neurofibromas. MPNST are generally observed in patients aged between 20 and 50 years [44]. MPNST are typically aggressive and have poor clinical outcomes [45].

^{18}F-FDG PET demonstrates moderate to strong uptake, as reflected by increased metabolism in malignant cells

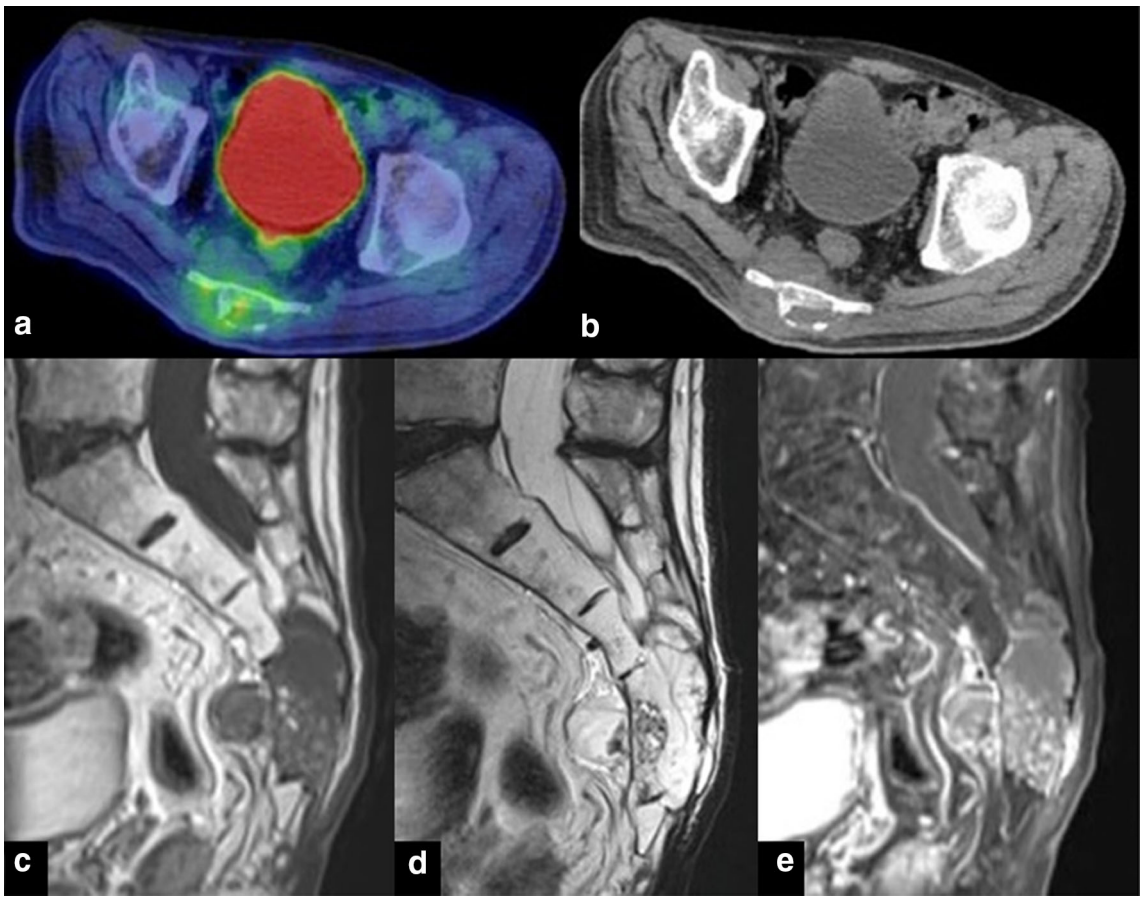

Fig. 4 A 70-year-old male with chordoma of the sacrum. **a** ^{18}F-FDG PET/CT shows heterogeneous and mild uptake with SUVmax of 1.7. **b** CT shows a bone destructive tumor. **c**–**e** MRI shows hypointensity with hyperintense foci on T1WI, heterogenous hyperintensity with a septal rim on T2WI, and heterogeneous enhancement on Gd-enhanced T1WI

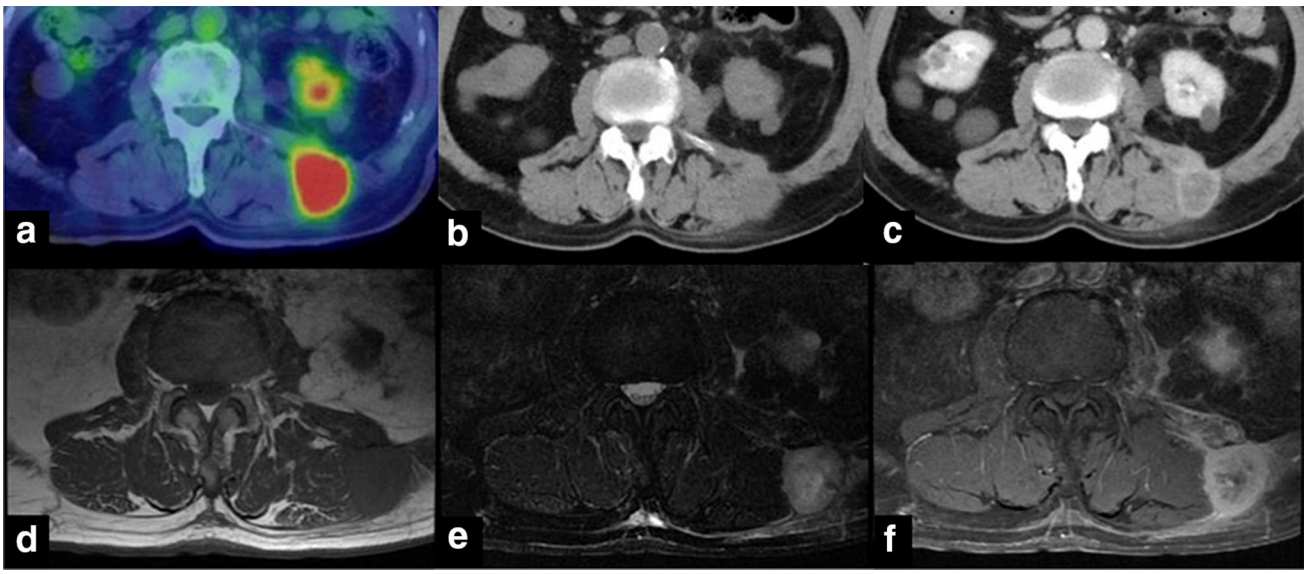

Fig. 5 An 81-year-old male with leiomyosarcoma in the left erector spinae muscles. **a** ^{18}F-FDG PET/CT demonstrates strong uptake with SUVmax of 8.3. **b**, **c** CT images show a poorly marginated soft tissue attenuation mass and heterogeneous enhancement. **d**–**f** MRI reveals isointensity to the muscle on T1WI, heterogeneous hyperintensity on T2WI, and heterogeneous enhancement on Gd-enhanced T1WI

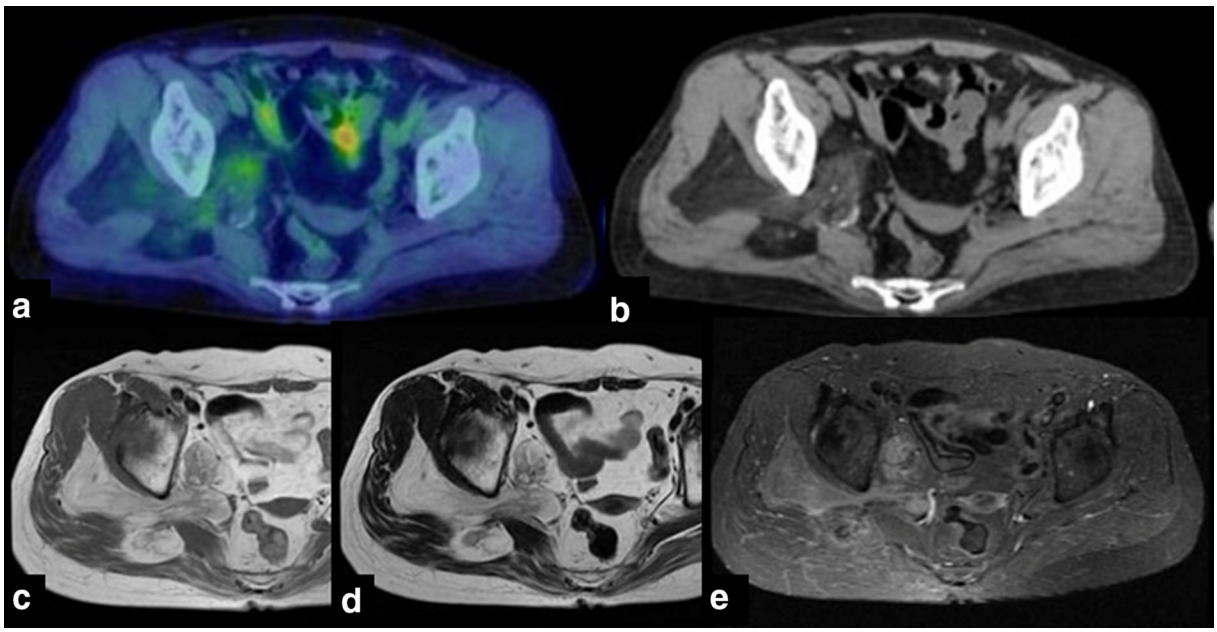

Fig. 6 A 73-year-old male with a well-differentiated liposarcoma in the pelvis and buttock. **a** ^{18}F-FDG PET/CT demonstrates heterogeneous and mild uptake with SUVmax of 2.1. **b** CT shows a heterogeneous fatty tumor with calcified foci. **c–e** MRI reveals a heterogenous fatty signal intensity mass

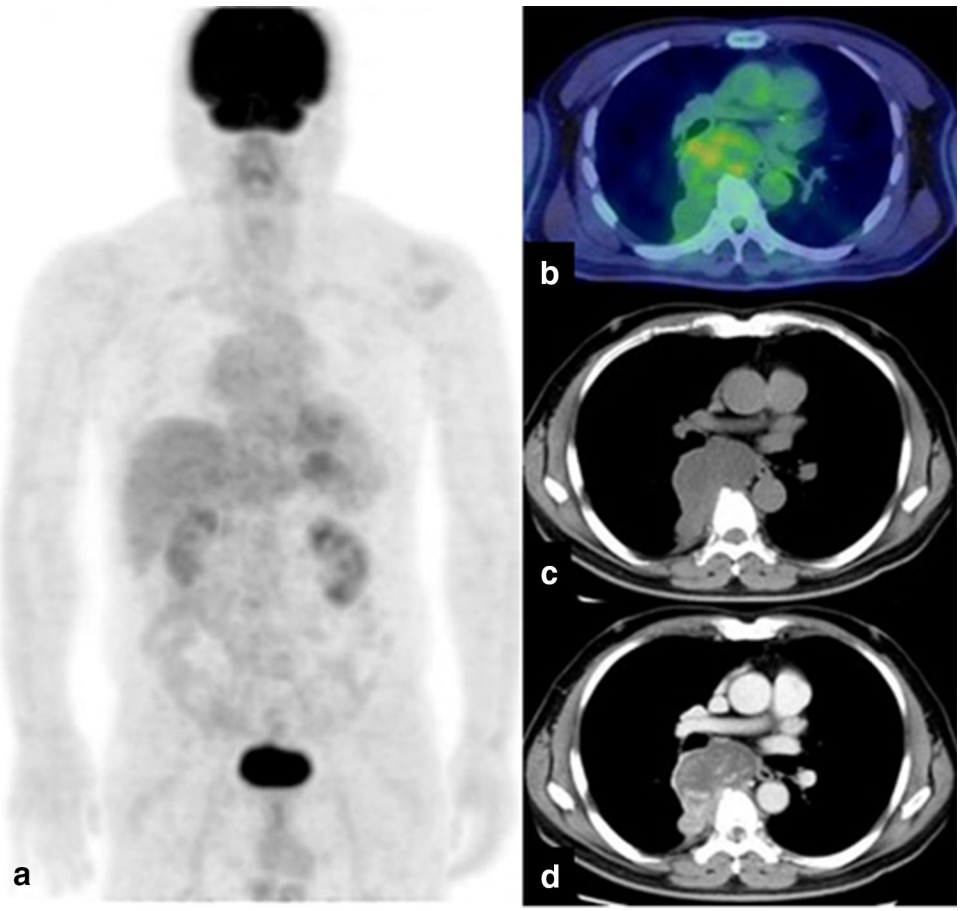

Fig. 7 A 65-year-old male with myxoid liposarcoma in the posterior mediastinum. **a**, **b** ^{18}F-FDG PET/CT and MIP images demonstrate heterogeneous and moderate uptake with SUVmax of 2.4. **c**, **d** CT shows a low attenuation mass with heterogeneous enhancement

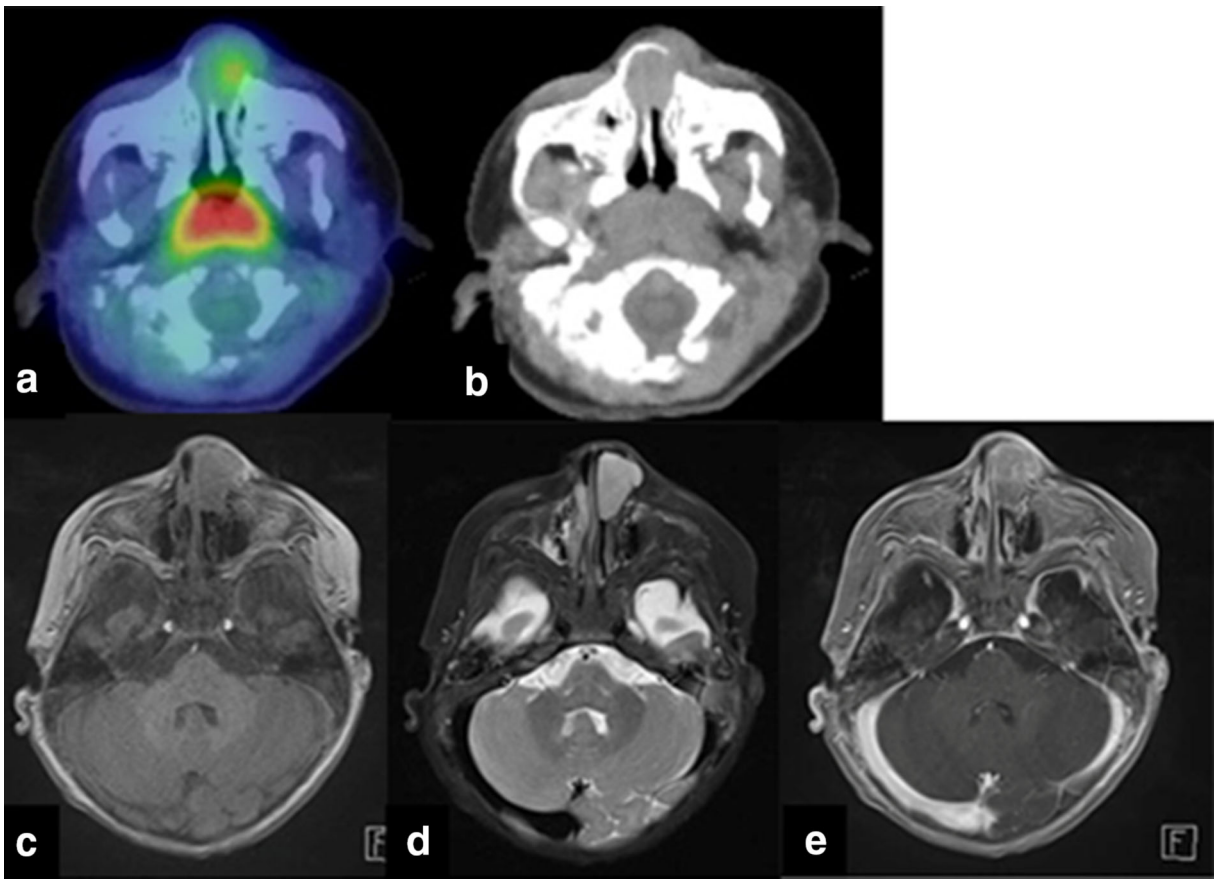

Fig. 8 A 4-month-old boy with rhabdomyosarcoma of the nasal cavity. **a** ^{18}F-FDG PET/CT demonstrates moderate uptake with SUVmax of 2.2. **b** CT shows an osteolytic soft tissue attenuation mass. **c–e** MRI demonstrates intermediate intensity on T1WI, hyperintensity on T2WI, and heterogeneous, mild enhancement on Gd-enhanced T1WI

[45–47] (Fig. 12). Khiewan et al. reported that ^{18}F-FDG PET/CT provided more accurate diagnostic performance than conventional imaging for staging and restaging, resulting in changes in treatment plans [47].

CT shows these tumors as heterogeneous low attenuation and heterogeneous enhancement reflecting necrosis, hemorrhage, or cystic degeneration [44]. MRI reveals these tumors as intermediate to hypointensity on T1WI, and as heterogeneous hyperintensity on T2WI, consistent with cystic or necrotic degeneration [26, 44, 45]. The imaging findings of MPNST include rapid growth, a large size, infiltrative margins, irregular peripheral enhancement with central necrosis, and peritumoral edema [26].

Benign tumors and tumor-like conditions

Intraosseous hemangioma

Intraosseous hemangioma is a benign and slow-growing vascular malformation of an endothelial origin [1]. Histologically, hemangiomas have been classified as capillary, cavernous, venous, or mixed according to the predominant vessel type. Cavernous hemangioma is the most common type [48]. Intraosseous hemangioma is most commonly located in the vertebra (particularly, the thoracic vertebra) and skull [1].

Most cases of ^{18}F-FDG PET/CT show no or faint uptake, reflecting metabolically stable benign tumors [1, 48, 49] (Fig. 13). Hatayama et al. reported that the SUVmax of hemangioma, including osseous and soft tissues, ranged between 0.7 and 1.6 on ^{18}F-FDG PET/CT in 16 hemangiomas [49]. In contrast, moderate to strong uptakes are sometimes reported (Fig. 14), and the SUVmax of hemangioma ranged between 4.7 and 5.5 in previous case reports [48, 50, 51]. Although the reason for increased uptake remains unclear, ^{18}F-FDG uptake may reflect internal hemorrhage accompanied by inflammation [51].

CT typically shows these tumors to have the lobular architecture of osteolytic lesions as well as coarse trabeculation and matrix mineralization [50]. MRI findings of intraosseous hemangiomas vary according to the proportion of vascular and lipomatous soft tissue elements. Signal intensities on T1WI and T2WI increase as the amount of

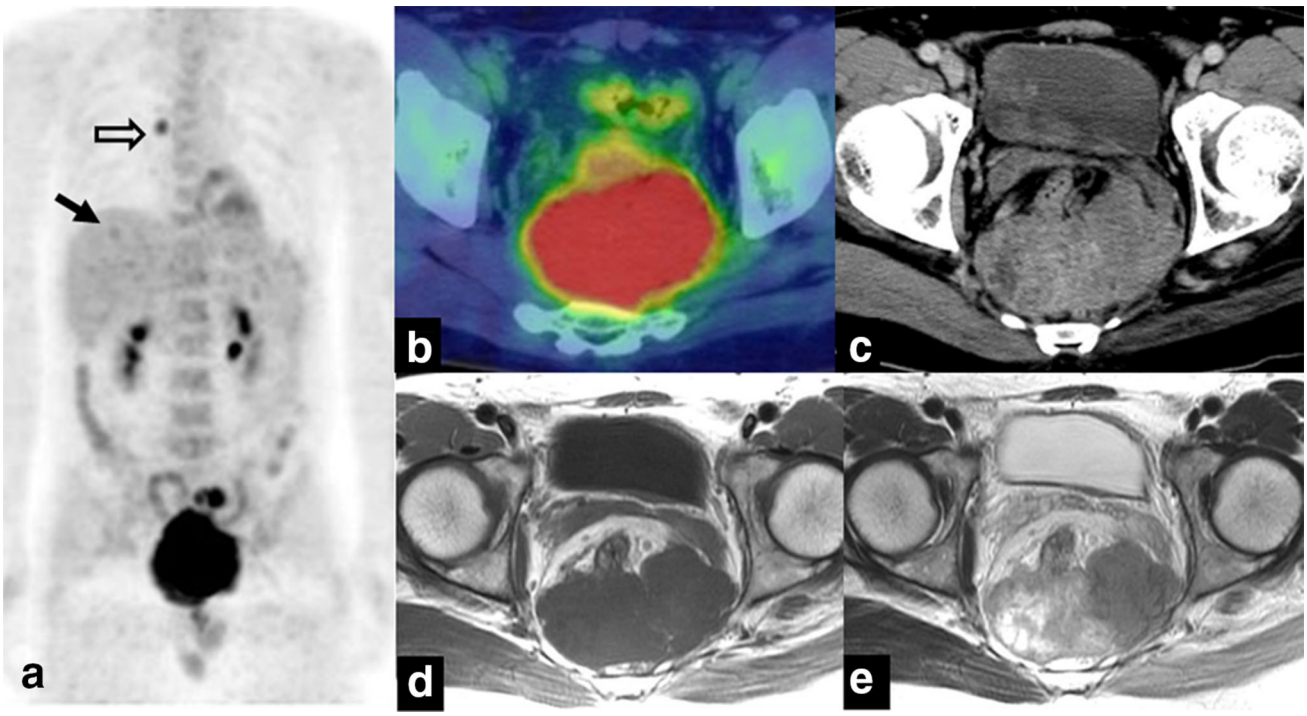

Fig. 9 A 42-year-old male with a desmoplastic small round cell tumor of the pelvis. **a**, **b** ^{18}F-FDG PET/CT and MIP images demonstrate strong uptake with SUVmax of 8.5. An MIP image shows mediastinal lymph node metastasis (*open arrow*) and liver metastasis (*arrow*). **c** Contrast-enhanced CT shows a heterogeneously enhanced mass. **d**, **e** MRI demonstrates hypointensity on T1WI and heterogeneous hyperintensity on T2WI

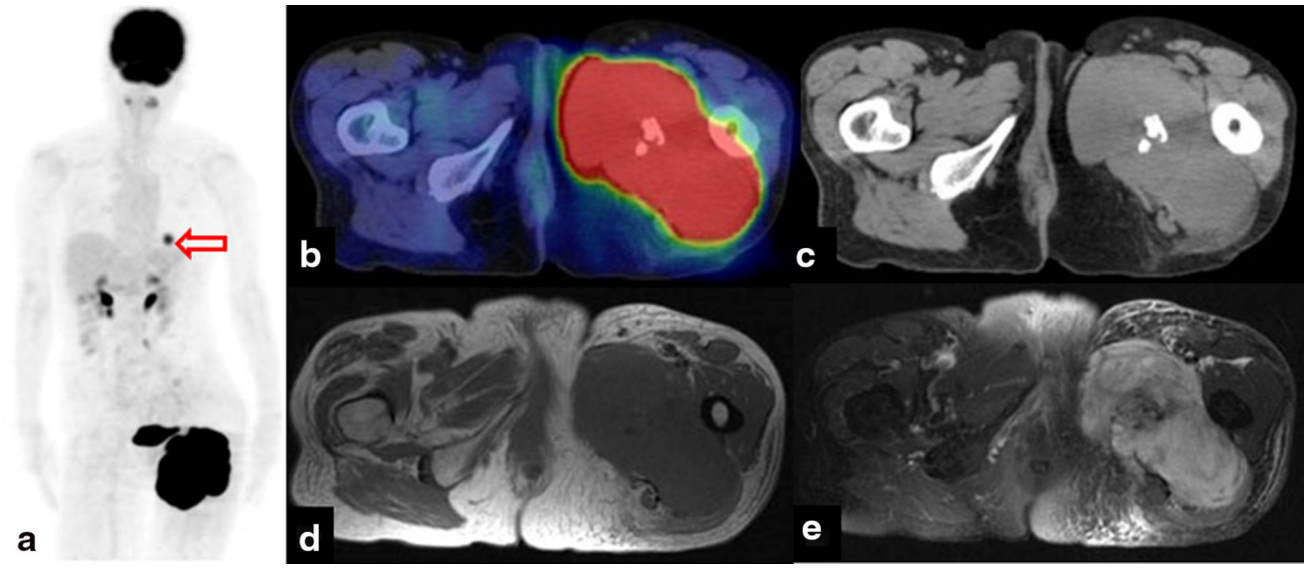

Fig. 10 A 74-year-old female with undifferentiated sarcoma of the left thigh. **a**, **b** ^{18}F-FDG PET/CT and MIP images demonstrate strong uptake with SUVmax of 36.2. An MIP image shows pulmonary metastasis (*open arrow*). **c** CT shows a soft tissue attenuation mass with calcification. **d**, **e** MRI reveals hypointensity on T1WI and heterogeneous hyperintensity on FS-T2WI

the fat component becomes larger, whereas these tumors show hypointensity on T1WI and hyperintensity on T2WI with the primary composition of vascular structures. Gd-enhanced T1WI shows variable degrees of enhancement [48, 50].

Enchondromas

Enchondromas are the second most common benign bone tumor and are characterized as solitary, benign, intramedullary cartilaginous tumors that most commonly

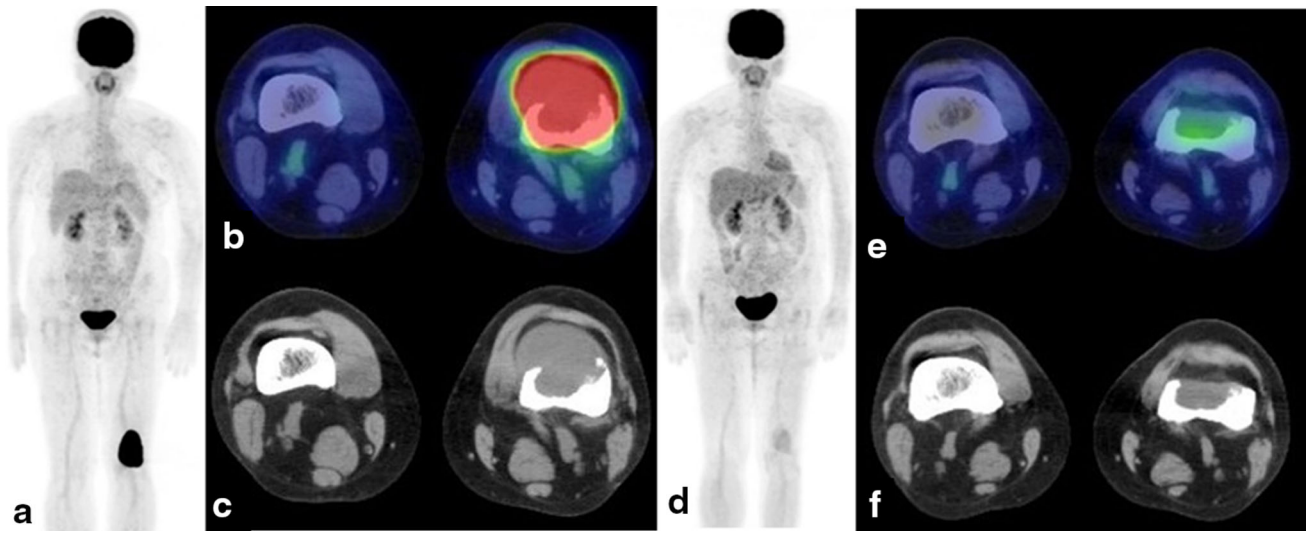

Fig. 11 A 44-year-old female with undifferentiated sarcoma of the lower end of the left femur. **a**, **b** ^{18}F-FDG PET/CT and MIP images demonstrate strong uptake with SUVmax of 48.1. **c** CT shows a soft tissue attenuation mass with bone destruction. **d**, **e** ^{18}F-FDG PET/CT and MIP images demonstrate mild uptake with SUVmax of 2.1, consistent with a complete treatment response. **f** CT shows shrinkage of the soft tissue mass; however, the tumor appears to be residual

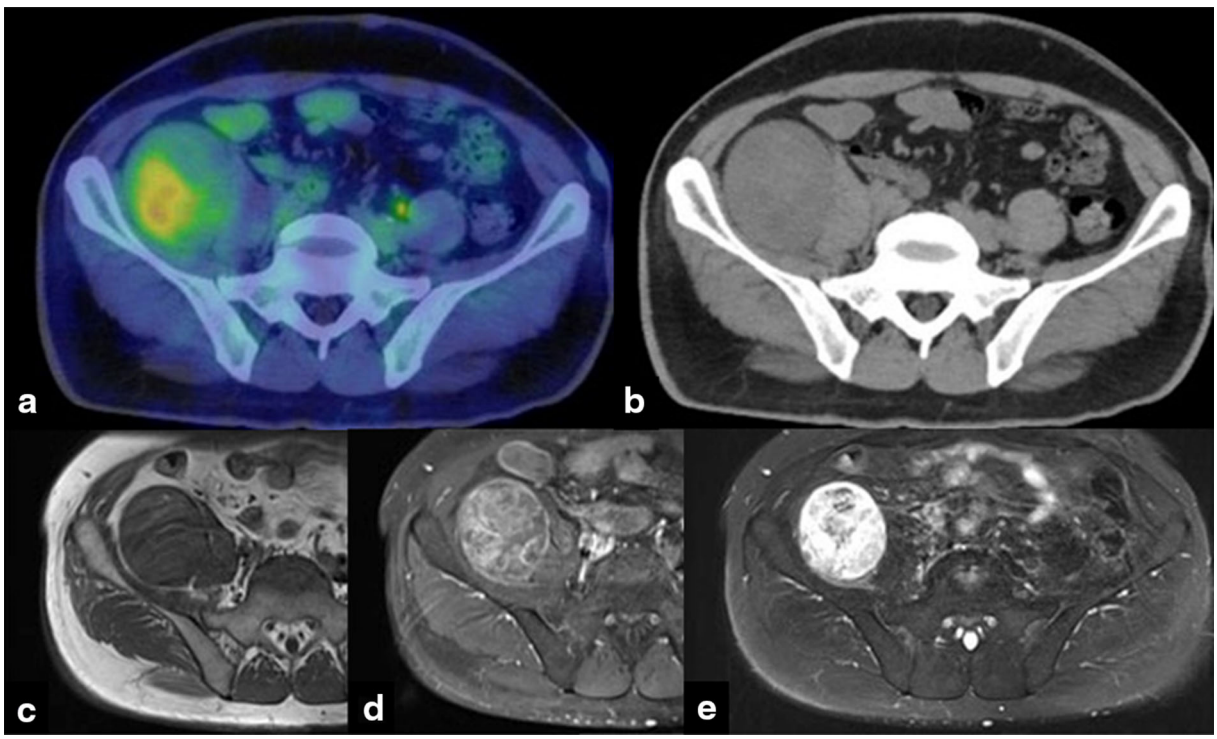

Fig. 12 A 52-year-old male with a malignant peripheral nerve sheath tumor of the right retroperitoneum. **a** ^{18}F-FDG PET/CT demonstrates heterogeneous and moderate uptake with SUVmax of 3.1. **b** CT shows a soft tissue attenuation mass. **c**–**e** MRI reveals hypointensity on T1WI, heterogeneous hyperintensity on T2WI, and heterogeneously enhancement on Gd-enhanced T1WI

occur in the small bones of the hands and feet. Enchondromas are generally observed between 20 and 40 years of age with equal gender distribution, being discovered incidentally in almost all cases [52]. The involvement of multiple growth plates is considered to result in enchondromatosis (Ollier disease and Maffucci syndrome) [52].

^{18}F-FDG PET/CT demonstrates mild uptake, and the SUVmax of enchondromas was previously reported to be lower than 3 [18, 19, 53] (Fig. 15).

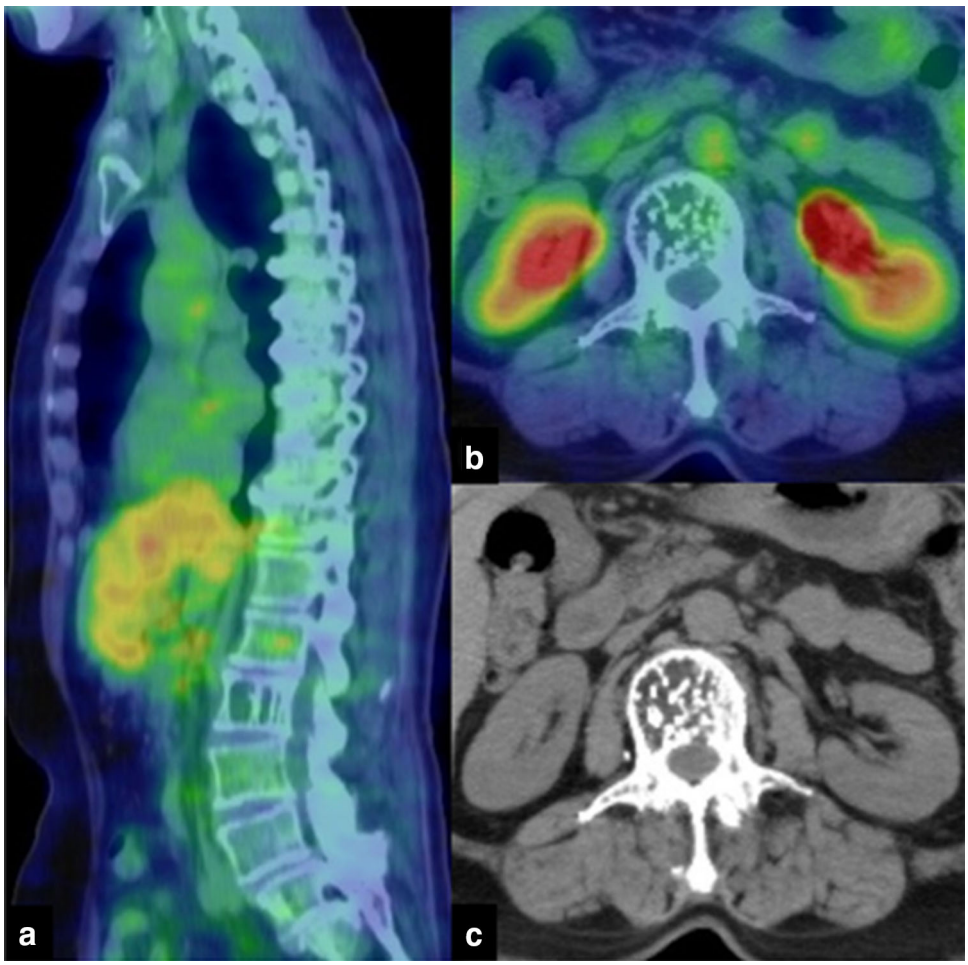

Fig. 13 A 70-year-old male with intraosseous hemangioma of the lumbar vertebra. **a**, **b** ^{18}F-FDG PET/CT demonstrates mild uptake with SUVmax of 1.7. **c** CT shows the typical findings of hemangioma, a multi-lobulated osteolytic lesion with sclerotic foci

CT shows these tumors as small osteolytic lesions with non-aggressive features, typically with ring and arc calcifications [4]. On MRI, these tumors typically have lobular contours with intermediate intensity on T1WI and hyperintensity on T2WI, consistent with hyaline cartilage [52].

Neurogenic tumors

Benign peripheral neurogenic tumors including schwannomas and neurofibromas are well-demarcated, round, or fusiform lesions located on the course of the peripheral nerve [2].

^{18}F-FDG PET/CT demonstrates mild uptake, or often strong uptake based on cell density [1, 54, 55] (Fig. 16).

CT shows these tumors as well-defined masses that are homogenous and soft tissue attenuation masses [44, 56]. MRI reveals these tumors as intermediate to hypointensity on T1WI and central hypointensity with peripheral hyperintensity on T2WI, which is often referred to as the target appearance. Gd-enhanced T1WI shows central enhancement and target signs [45, 56]. Imaging findings of schwannomas and neurofibromas are similar, and, thus, cannot be distinguished in most cases.

Langerhans cell histiocytosis

Langerhans cell histiocytosis (LCH) is a rare disease of unknown etiology that is characterized by abnormal clonal proliferation and the accumulation of pathological Langerhans cells in the involved regions, which are often organized in granulomas [57, 58]. LCH may occur in patients of all ages, with most patients being children [59]. LCH may affect any organ, with bone lesions being the most frequent manifestation of the disease [57]. Bone lesions have been reported in the skull and flat bones, and are often present with localized painful swelling [57, 61].

^{18}F-FDG PET/CT shows bone lesions uptake as strong as that of malignant bone tumors [57–60] (Fig. 17). ^{18}F-FDG PET/CT is useful for the detection of all the dissemination throughout the body and provides more clear demonstration of soft tissue involvement such as in the lymph nodes, lungs, or spleen. However, healed lesions may appear non-^{18}F-FDG avid [57, 58].

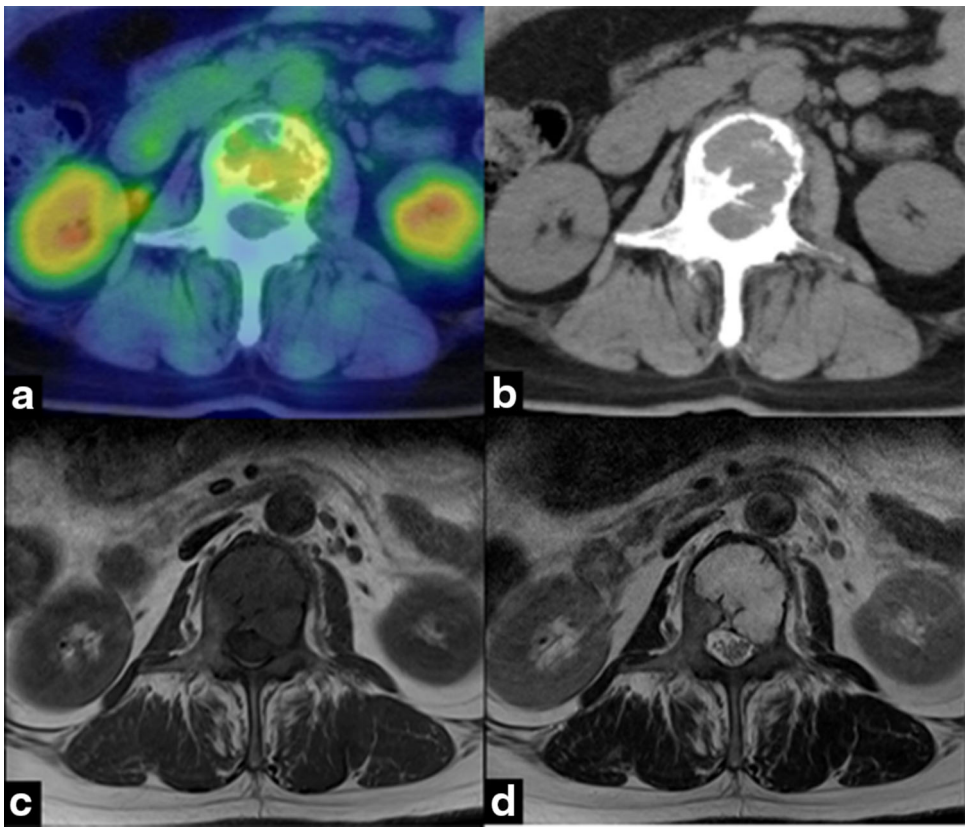

Fig. 14 A 62-year-old female with vertebral hemangioma of the lumbar vertebra confirmed by biopsy. **a** ^{18}F-FDG PET/CT demonstrates moderate uptake with SUVmax of 2.8. **b** CT shows a multi-lobulated osteolytic lesion and sclerotic column. **c**, **d** MRI reveals mild hypointensity on T1WI and hyperintensity on T2WI

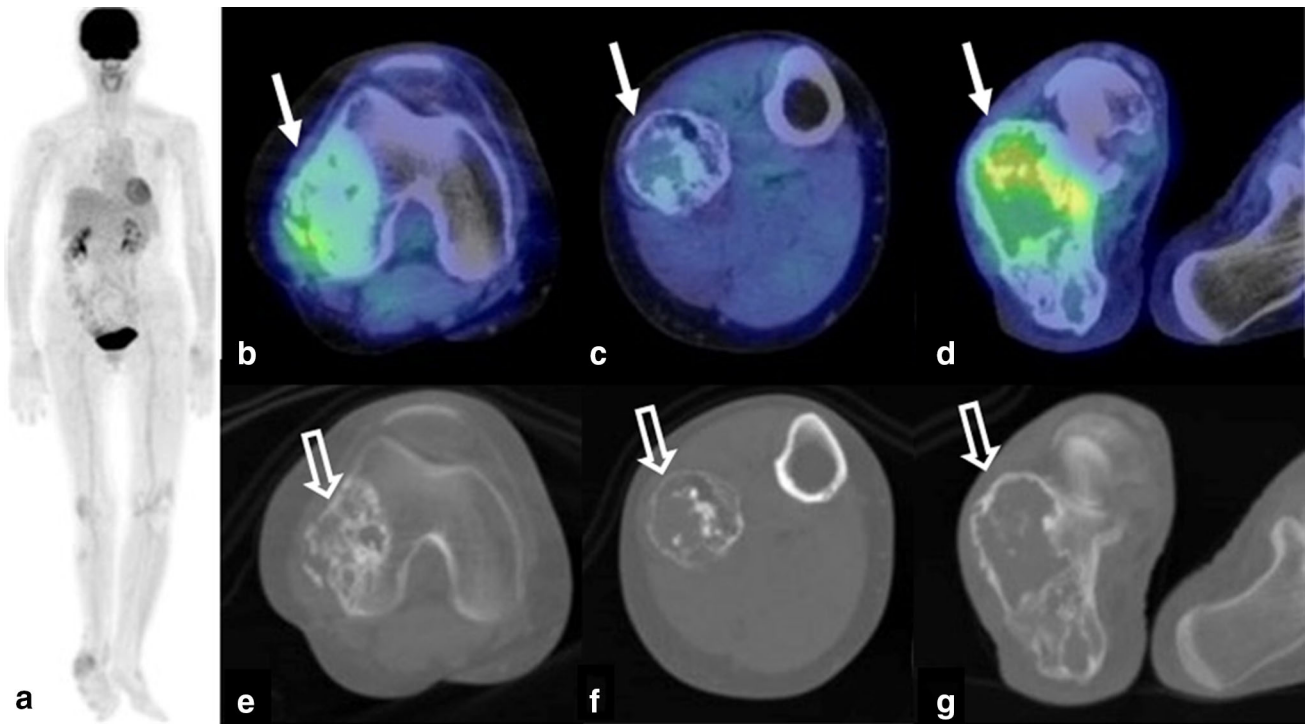

Fig. 15 A 74-year-old male with enchondromatosis (Ollier disease) of the right femur and tibia. **a**–**d** ^{18}F-FDG PET/CT and MIP images demonstrate mild to moderate uptake with SUVmax between 1.3 and 2.6. **e**–**g** CT shows osteolytic lesions with calcification

Fig. 16 A 64-year-old male with schwannoma of the left abdominal wall. **a** ^{18}F-FDG PET/CT demonstrates mild uptake with SUVmax of 1.8 (*arrow*). **b**, **c** CT shows a soft tissue attenuation mass with central enhancement (*open arrow*)

CT shows bone lesions as osteolytic lesions and soft tissue involvement [57–60]. MRI typically reveals these lesions as hypointensity on T1WI and hyperintensity on T2WI [61].

Fat necrosis

Fat necrosis is a sterile inflammatory process. Although its etiology is often unclear, there are several causes such as infection, trauma, ischemia, and surgical procedures [62].

^{18}F-FDG PET/CT demonstrates variable increased uptake (Fig. 18). Focal ^{18}F-FDG avid nodular changes are recognized because of the presence of metabolically active inflammatory cells [62, 63].

CT shows these lesions as nodular lesions with greater hypoattenuation than soft tissue, varying between −50 and 30 HU in most cases [63]; however, CT findings vary with the ages of the lesions. On MRI, fat necrosis shows hypointensities on T1WI and T2WI as a result of iron-containing siderophages, surrounded by a rim of variable signal intensity that may represent surrounding edema. Intense signals from fat in lesions may be useful for the diagnosis of fat necrosis. Gd-enhanced T1WI shows a variable appearance because of the various stages in the development, maturation, and resolution of fat necrosis [62].

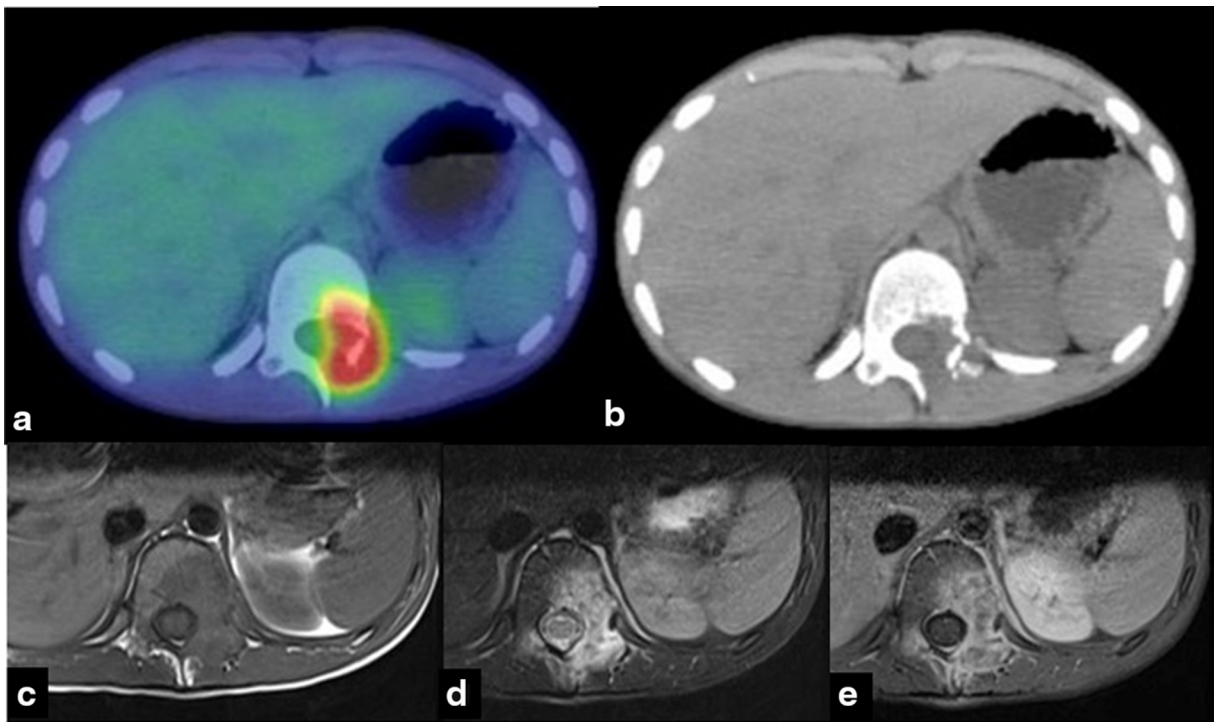

Fig. 17 A 14-year-old male with Langerhans cell histiocytosis. **a** ^{18}F-FDG PET/CT demonstrates strong uptake with SUVmax of 5.9. **b** CT shows soft tissue in the left vertebral arch with bony destruction. **c**–**e** MRI reveals hypointensity on T1WI, heterogenous hyperintensity on fat-suppressed T2WI, and heterogeneous enhancement on Gd-enhanced T1WI

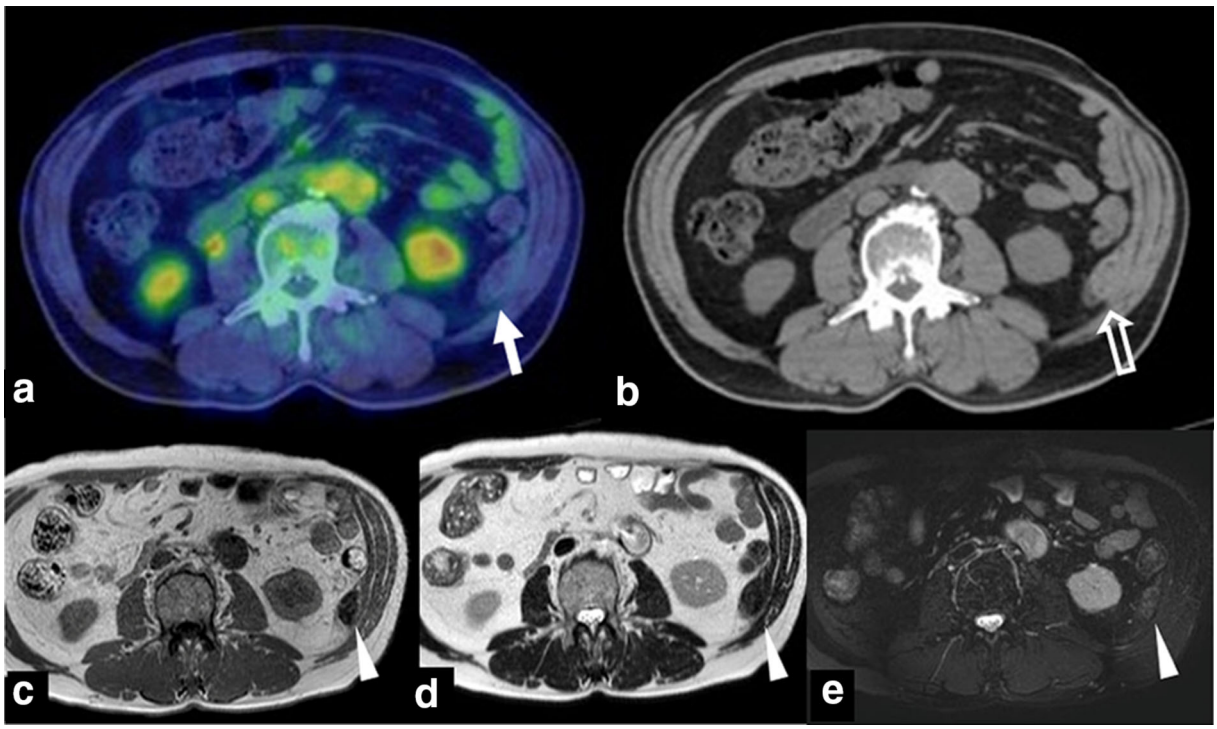

Fig. 18 A 72-year-old male with fat necrosis of the abdominal wall. **a** ^{18}F-FDG PET/CT demonstrates mild uptake with SUVmax of 1.1 (*arrow*). **b** CT shows a heterogeneous soft tissue attenuation mass with small fat attenuation (*open arrow*). **c–e** MRI reveals hypointensity on T1WI and T2WI with small fat signal intensity, and heterogeneous and mild hyperintensity on FS-T2WI (*arrowheads*)

Evaluation of ^{18}F-FDG uptake

In clinical practice, SUVmax is widely used as a semi-quantitative parameter and useful indicator of tumor aggressiveness and prognosis indicator in a variety of malignant tumors including musculoskeletal tumors. However, SUVmax only represents the single greatest point of metabolic activity within the tumor; it cannot be used to evaluate the entire metabolic tumor burden. Recently, some studies reported the usefulness of volumetric analysis using metabolic tumor volume (MTV) and total lesion glycolysis (TLG) which indicate metabolic activity throughout the tumor volume in therapeutic response and prognostication in malignant musculoskeletal tumors [64–66]. However, there is as yet no standardized method and suitable SUV threshold for volumetric analysis.

Non-FDG tracers

^{18}F-FDG is a tracer of increased intracellular glucose metabolism and not specific for malignant tumor. Besides ^{18}F-FDG, based on different mechanisms and clinical issues, some PET compounds such as ^{11}C-methionine as amino acid tracer and ^{18}F-fluorothimidine (FLT) for proliferation marker, ^{18}F-sodium fluoride as bone-imaging agent, and ^{18}F-garacto-RGD as biomarkers of neoangiogenesis are currently under investigation for staging, grading, detection of recurrence, and assessment of therapeutic response in malignant musculoskeletal tumors [67, 68].

Conclusions

^{18}F-FDG PET/CT is increasingly being used to evaluate musculoskeletal tumors and plays an important role in the staging, tumor grading, evaluation of treatment responses, and detection of recurrence in malignant tumors. Although musculoskeletal tumors show various ^{18}F-FDG uptakes on PET/CT, its addition to morphological imaging modalities such as CT and MRI is useful for the characterization and differentiation of musculoskeletal lesions.

References

1. Choi YY, Kim JY, Yang SO. PET/CT in benign and malignant musculoskeletal tumors and tumor-like conditions. Semin Musculoskelet Radiol. 2014;18:133–48.

2. Sheikhbahaei S, Marcus C, Hafezi-Nejad N, Taghipour M, Subramaniam RM. Value of FDG PET/CT in patient management and outcome of skeletal and soft tissue sarcomas. PET Clin. 2015;10:375–93.
3. Brenner W, Bohuslavizki KH, Eary JF. PET imaging of osteosarcoma. J Nucl Med. 2003;44:930–42.
4. Costelloe CM, Chuang HH, Madewell JE. FDG PET/CT of primary bone tumors. AJR Am J Roentgenol. 2014;202:W521–31.
5. Even-Sapir E. PET/CT in malignant bone disease. Semin Musculoskelet Radiol. 2007;11:312–21.
6. Quartuccio N, Treglia G, Salsano M, Mattoli MV, Muoio B, Piccardo A, et al. The role of fluorine-18-fluorodeoxyglucose positron emission tomography in staging and restaging of patients with osteosarcoma. Radiol Oncol. 2013;47:97–102.
7. Byun BH, Kong CB, Park J, Seo Y, Lim I, Choi CW, et al. Initial metabolic tumor volume measured by ^{18}F-FDG PET/CT can predict the outcome of osteosarcoma of the extremities. J Nucl Med. 2013;54:1725–32.
8. Rakheja R, Makis W, Skamene S, Nahal A, Brimo F, Azoulay L, et al. Correlating metabolic activity on ^{18}F-FDG PET/CT with histopathologic characteristics of osseous and soft-tissue sarcomas: a retrospective review of 136 patients. AJR Am J Roentgenol. 2012;198:1409–16.
9. Folpe AL, Lyles RH, Sprouse JT, Conrad EU 3rd, Eary JF. (F-18) fluorodeoxyglucose positron emission tomography as a predictor of pathologic grade and other prognostic variables in bone and soft tissue sarcoma. Clin Cancer Res. 2000;6:1279–87.
10. Eary JF, Conrad EU, Bruckner JD, Folpe A, Hunt KJ, Mankoff DA, et al. Quantitative [F-18]fluorodeoxyglucose positron emission tomography in pretreatment and grading of sarcoma. Clin Cancer Res. 1998;4:1215–20.
11. Hongtao L, Hui Z, Bingshun W, Xiaojin W, Zhiyu W, Shuier Z, et al. 18F-FDG positron emission tomography for the assessment of histological response to neoadjuvant chemotherapy in osteosarcomas: a meta-analysis. Surg Oncol. 2012;21:e165–70.
12. Kong CB, Byun BH, Lim I, Choi CW, Lim SM, Song WS, et al. ^{18}F-FDG PET SUVmax as an indicator of histopathologic response after neoadjuvant chemotherapy in extremity osteosarcoma. Eur J Nucl Med Mol Imaging. 2013;40:728–36.
13. Peller PJ. Role of positron emission tomography/computed tomography in bone malignancies. Radiol Clin N Am. 2013;51:845–64.
14. Quartuccio N, Fox J, Kuk D, et al. Pediatric bone sarcoma: diagnostic performance of ^{18}F-FDG PET/CT versus conventional imaging for initial staging and follow-up. AJR Am J Roentgenol. 2015;204:153–60.
15. Thornton E, Krajewski KM, O'Regan KN, Giardino AA, Jagannathan JP, Ramaiya N. Imaging features of primary and secondary malignant tumours of the sacrum. Br J Radiol. 2012;85:279–86.
16. Douis H, Saifuddin A. The imaging of cartilaginous bone tumours. II. Chondrosarcoma. Skelet Radiol. 2013;42:611–26.
17. Brenner W, Conrad EU, Eary JF. FDG PET imaging for grading and prediction of outcome in chondrosarcoma patients. Eur J Nucl Med Mol Imaging. 2004;31:189–95.
18. Aoki J, Watanabe H, Shinozaki T, Tokunaga M, Inoue T, Endo K. FDG-PET in differential diagnosis and grading of chondrosarcomas. J Comput Assist Tomogr. 1999;23:603–8.
19. Jesus-Garcia R, Osawa A, Filippi RZ, Viola DC, Korukian M, de Carvalho Campos Neto G, et al. Is PET-CT an accurate method for the differential diagnosis between chondroma and chondrosarcoma? Springerplus. 2016;5:236.
20. Miyazawa N, Ishigame K, Kato S, Satoh Y, Shinohara T. Thoracic chordoma: review and role of FDG-PET. J Neurosurg Sci. 2008;52:117–21.
21. Mammar H, Kerrou K, Nataf V, Pontvert D, Clemenceau S, Lot G, et al. Positron emission tomography/computed tomography imaging of residual skull base chordoma before radiotherapy using fluoromisonidazole and fluorodeoxyglucose: potential consequences for dose painting. Int J Radiat Oncol Biol Phys. 2012;84:681–7.
22. Park SA, Kim HS. F-18 FDG PET/CT evaluation of sacrococcygeal chordoma. Clin Nucl Med. 2008;33:906–8.
23. Ochoa-Figueroa MA, Martínez-Gimeno E, Allende-Riera A, Cabello-García D, Muñoz-Iglesias J, Cárdenas-Negro C. Role of 18F-FDG PET-CT in the study of sacrococcygeal chordoma. Rev Esp Med Nucl Imagen Mol. 2012;31:359–61.
24. O'Sullivan PJ, Harris AC, Munk PL. Radiological imaging features of non-uterine leiomyosarcoma. Br J Radiol. 2008;81:73–81.
25. Punt SE, Eary JF, O'Sullivan J, Conrad EU. Fluorodeoxyglucose positron emission tomography in leiomyosarcoma: imaging characteristics. Nucl Med Commun. 2009;30:546–9.
26. Jagannathan JP, Tirumani SH, Ramaiya NH. Imaging in soft tissue sarcomas: current updates. Surg Oncol Clin N Am. 2016;25:645–75.
27. Tewfik JN, Greene GS. Fluorine-18-deoxyglucose-positron emission tomography imaging with magnetic resonance and computed tomographic correlation in the evaluation of bone and soft-tissue sarcomas: a pictorial essay. Curr Probl Diagn Radiol. 2008;37:178–88.
28. Crago AM, Dickson MA. Liposarcoma: multimodality management and future targeted therapies. Surg Oncol Clin N Am. 2016;25:761–73.
29. Murphey MD, Arcara LK, Fanburg-Smith J. From the archives of the AFIP: imaging of musculoskeletal liposarcoma with radiologic–pathologic correlation. Radiographics. 2005;25:1371–95.
30. Brenner W, Eary JF, Hwang W, Vernon C, Conrad EU. Risk assessment in liposarcoma patients based on FDG PET imaging. Eur J Nucl Med Mol Imaging. 2006;33:1290–5.
31. Evilevitch V, Weber WA, Tap WD, Allen-Auerbach M, Chow K, Nelson SD, et al. Reduction of glucose metabolic activity is more accurate than change in size at predicting histopathologic response to neoadjuvant therapy in high-grade soft-tissue sarcomas. Clin Cancer Res. 2008;14:715–20.
32. Saboo SS, Krajewski KM, Zukotynski K, Howard S, Jagannathan JP, Hornick JL, et al. Imaging features of primary and secondary adult rhabdomyosarcoma. AJR Am J Roentgenol. 2012;199:W694–703.
33. Dong Y, Zhang X, Wang S, Chen S, Ma C. 18[F]FDG PET/CT is useful in initial staging, restaging for pediatric rhabdomyosarcoma. Q J Nucl Med Mol Imaging. 2015 **(epub ahead of print)**.
34. Van Rijn RR, Wilde JC, Bras J, Oldenburger F, McHugh KM, Merks JH. Imaging findings in noncraniofacial childhood rhabdomyosarcoma. Pediatr Radiol. 2008;38:617–34.
35. Federico SM, Spunt SL, Krasin MJ, Billup CA, Wu J, Shulkin B, et al. Comparison of PET-CT and conventional imaging in staging pediatric rhabdomyosarcoma. Pediatr Blood Cancer. 2013;60:1128–34.
36. Kis B, O'Regan KN, Agoston A, Javery O, Jagannathan J, Ramaiya NH. Imaging of desmoplastic small round cell tumour in adults. Br J Radiol. 2012;85:187–92.
37. Ostermeier A, McCarville MB, Navid F, Snyder SE, Shulkin BL. FDG PET/CT imaging of desmoplastic small round cell tumor: findings at staging, during treatment and at follow-up. Pediatr Radiol. 2015;45:1308–15.
38. Zhang WD, Li CX, Liu QY, Hu YY, Cao Y, Huang JH. CT, MRI, and FDG-PET/CT imaging findings of abdominopelvic desmoplastic small round cell tumors: correlation with histopathologic findings. Eur J Radiol. 2011;80:269–73.

39. Fletcher CDM, Bridge JA, Pancreas CW, Hogendoorn PCW, Mertens F. WHO Classification of tumours of soft tissue and bone. 4th ed. Lyon: IARC; 2013.
40. Sachpekidis C, Langer R, Kollàr A, Wartenberg J. Detection of a primary tumor in the area of the renal artery with 18F-FDG PET/CT in a patient with metastatic undifferentiated sarcoma and a history of mid-aortic syndrome: a case report. Medicine (Baltimore). 2016;95:e4622.
41. Wei WJ, Shen CT, Song HJ, Qiu ZL, Luo QY. Metastatic malignant fibrous histiocytoma infiltrating sigmoid colon: a case diagnosed with the help of 18F-FDG PET/CT. Clin Nucl Med. 2016;41:338–40.
42. Fang N, Wang YL, Zeng L, Wu ZJ, Cui XJ. Metastatic malignant fibrous histiocytoma in the stomach: imaging with 18F-FDG PET/CT. Clin Nucl Med. 2016;41:e123–4.
43. Li J, Geng ZJ, Lv XF, Zhang XK, Xie CM. Computed tomography and magnetic resonance imaging findings of malignant fibrous histiocytoma of the head and neck. Mol Clin Oncol. 2016;4:888–92.
44. Lin J, Martel W. Cross-sectional imaging of peripheral nerve sheath tumors: characteristic signs on CT, MR imaging, and sonography. AJR Am J Roentgenol. 2001;176:75–82.
45. Broski SM, Johnson GB, Howe BM, Nathan MA, Wenger DE, Spinner RJ, et al. Evaluation of ^{18}F-FDG PET and MRI in differentiating benign and malignant peripheral nerve sheath tumors. Skelet Radiol. 2016;45:1097–105.
46. Cardona S, Schwarzbach M, Hinz U, et al. Evaluation of F18-deoxyglucose positron emission tomography (FDG-PET) to assess the nature of neurogenic tumours. Eur J Surg Oncol. 2003;29:536–41.
47. Khiewan B, Macapinlac HA, Lev D, McCutcheon IE, Slopis JM, Al Sannaa G, et al. The value of ^{18}F-FDG PET/CT in the management of malignant peripheral nerve sheath tumors. Eur J Nucl Med Mol Imaging. 2014;41:1756–66.
48. Cha JG, Yoo JH, Kim HK, Park JM, Paik SH, Park SJ. PET/CT and MRI of intra-osseous haemangioma of the tibia. Br J Radiol. 2012;85:e94–8.
49. Hatayama K, Watanabe H, Ahmed AR, Yanagawa T, Shinozaki T, Oriuchi N, et al. Evaluation of hemangioma by positron emission tomography: role in a multimodality approach. J Comput Assist Tomogr. 2003;27:70–7.
50. Matsumoto Y, Takahashi Y, Haraguchi A. Intraosseous hemangioma arising in the clavicle. Skelet Radiol. 2014;43:89–93.
51. Nakayama M, Okizaki A, Ishitoya S, Aburano T. "Hot" vertebra on (18)F-FDG PET scan: a case of vertebral hemangioma. Clin Nucl Med. 2012;37:1190–3.
52. Douis H, Saifuddin A. The imaging of cartilaginous bone tumours. I. Benign lesions. Skelet Radiol. 2012;41:1195–212.
53. Mukherjee A, Singla S, Das CJ, Bal C, Kumar R. Enchondroma of clivus: appearance on ^{18}F-FDG PET-CT in contrast with MRI. Clin Nucl Med. 2015;40:e53–4.
54. Nose H, Otsuka H, Otomi Y, Terazawa K, Takao S, Iwamoto S, et al. Correlations between F-18 FDG PET/CT and pathological findings in soft tissue lesions. J Med Invest. 2013;60:184–90.
55. Miyake KK, Nakamoto Y, Kataoka TR, Ueshima C, Higashi T, Terashima T, et al. Clinical, morphologic, and pathologic features associated with increased FDG uptake in schwannoma. AJR Am J Roentgenol. 2016;207:1288–96.
56. Pilavaki M, Chourmouzi D, Kiziridou A, Skordalaki A, Zarampoukas T, Drevelengas A. Imaging of peripheral nerve sheath tumors with pathologic correlation: pictorial review. Eur J Radiol. 2004;52:229–39.
57. Agarwal KK, Seth R, Behra A, Jana M, Kumar R. 18F-Fluorodeoxyglucose PET/CT in Langerhans cell histiocytosis: spectrum of manifestations. Jpn J Radiol. 2016;34:267–76.
58. Obert J, Vercellino L, Van Der Gucht A, de Margerie-Mellon C, Bugnet E, Chevret S, et al. ^{18}F-fluorodeoxyglucose positron emission tomography–computed tomography in the management of adult multisystem Langerhans cell histiocytosis. Eur J Nucl Med Mol Imaging. 2017;44:598–610.
59. Long Q, Shaoyan W, Hui W. 18F-fluorodeoxyglucose positron emission tomography/computed tomography for primary thyroid Langerhans histiocytosis: a case report and literature review. Indian J Nucl Med. 2015;30:328–30.
60. Koç ZP, Şimşek S, Akarsu S, Balcı TA, Onur MR, Kepenek F. Insufficiency of bone scintigraphy in vertebral lesions of Langerhans cell histiocytosis compared to F-18 fluorodeoxyglucose positron emission tomography/computed tomography and diagnostic computed tomography. Mol Imaging Radionucl Ther. 2015;24:21–4.
61. Pavlik M, Bloom DA, Ozgönenel B, Sarnaik SA. Defining the role of magnetic resonance imaging in unifocal bone lesions of Langerhans cell histiocytosis. J Pediatr Hematol Oncol. 2005;27:432–5.
62. Adejolu M, Huo L, Rohren E, Santiago L, Yang WT. False-positive lesions mimicking breast cancer on FDG PET and PET/CT. AJR Am J Roentgenol. 2012;198:W304–14.
63. Kashyap R, Lau E, George A, Seymour JF, Lade S, Hicks RJ, et al. High FDG activity in focal fat necrosis: a pitfall in interpretation of posttreatment PET/CT in patients with non-Hodgkin lymphoma. Eur J Nucl Med Mol Imaging. 2013;40:1330–6.
64. Im HJ, Kim TS, Park SY, Min HS, Kim JH, Kang HG, et al. Prediction of tumour necrosis fractions using metabolic and volumetric 18F-FDG PET/CT indices, after one course and at the completion of neoadjuvant chemotherapy, in children and young adults with osteosarcoma. Eur J Nucl Med Mol Imaging. 2012;39:39–49.
65. Chen L, Wu X, Ma X, Guo L, Zhu C, Li Q. Prognostic value of 18F-FDG PET-CT-based functional parameters in patients with soft tissue sarcoma: a meta-analysis. Medicine (Baltimore). 2017;96:e5913.
66. Li YJ, Dai YL, Cheng YS, Zhang WB, Tu CQ. Positron emission tomography (18)F-fluorodeoxyglucose uptake and prognosis in patients with bone and soft tissue sarcoma: a meta-analysis. Eur J Surg Oncol. 2016;42:1103–14.
67. Kaste S. Imaging pediatric bone sarcomas. Radiol Clin N Am. 2011;49:749–65.
68. Wieder HA, Pomykala KL, Benz MR, Buck AK, Herrmann K. PET tracers in musculoskeletal disease beyond FDG. Semin Musculoskelet Radiol. 2014;18:123–32.